

Towards an exact approach to pulsar timing

Amodio Carleo ^{1,*} Delphine Perrodin,¹ and Andrea Possenti¹

¹*INAF, Osservatorio Astronomico di Cagliari, Via della Scienza 5, 09047 Selargius (CA), Italy*
(Dated: December 16, 2024)

The pulsar timing technique, which compares the observed arrival times of electromagnetic radiation from a pulsar with the predicted arrival times derived from a theoretical model of the pulsar system, is used in pulsar astronomy to infer a multitude of physical information and to constrain possible corrections to General Relativity (GR). The propagation delay is usually computed using formulas based on a post-Newtonian approach, for both the light trajectory and the orbital motion. However, evidence has recently emerged that this approximation may no longer be sufficient when the companion object is a supermassive black hole; deviations from a full GR computation of the propagation delay can reach a few seconds. In this paper, we analyze the case of binary pulsars with a stellar or intermediate black hole companion, whose discovery and timing are key goals of SKA. With a numerical algorithm, we have found that in this case, the full GR value depends only on the semi-major axis of the relative orbit and on the mass of the black hole companion. If the mass of the latter is sufficiently large ($100M_{\odot}$), the maximum difference between the two approaches is significant ($\sim 10^{-7}$ s) even for large binaries ($\sim 10^{16}$ cm), and increases up to $\sim 10^{-4}$ s when the mass is 10^5M_{\odot} . We also consider relativistic corrections to the orbital motion, and discover that they can strongly affect the value of the propagation delay. We conclude that in the future, post-Newtonian formulas should be replaced with a more accurate approach in these systems, especially in view of future discoveries made by new large telescopes such as SKA.

I. INTRODUCTION

Neutron stars are compact objects that are formed following the explosion of massive stars. Radio pulsars are neutron stars that emit beams of radio waves, which are detected at Earth's radio telescopes as extremely regular series of 'pulses', corresponding to the extremely regular rotation period of pulsars. The emitted energy, although predominant in the radio band, is actually broadband, with energies up to the GeV range and sometimes even in the TeV range. In some cases, pulsations appear in different energy bands, even if peaks in different bands may be associated with different emitting regions [40]. Since they are remarkably precise clocks, pulsars can be used to investigate many different aspects of physics, from the interior of neutron stars (NS) [3], to GR tests [15, 41], the density of the interstellar medium [23], dark matter [38] and the gravitational wave background (GWB) [44]. Most of the aforementioned studies involve the so-called "pulsar timing" technique, i.e. the measurement of the times-of-arrival (ToAs) of the radio signals emitted by the pulsar, which are then compared to the TOAs predicted by a theoretical model that accounts for many astrophysical processes involving the pulse's emission, among which: the pulsar system dynamics (e.g. pulsar spin, proper motion, etc.), solar system dynamics (e.g. motion of the Earth and planets), and the effects of the interstellar medium (e.g. dispersion and scintillation) or solar wind effects. Depending on whether the pulsar is isolated or in a binary, this multi-parameter fit gives several important parameters (the so-called ephemeris), such as the spin period, spin period

derivative, orbital period (if in a binary), position in the sky, eccentricity, etc. Currently, the pulsar community uses three main data analysis packages to analyze ToAs, namely TEMPO [34], TEMPO2 [18] and PINT [33]. Since the latter was written completely independently, it offers an excellent tool for cross-checking the output. This is becoming necessary, since for high-impact precision timing programs, such as gravitational wave detection efforts, it is critical to compare results from more than one single data analysis pipeline.

The first hint of the power of this method was seen in the case of the binary system PSR B1913+16, whose orbital decay agrees with the predicted GR values to better than 0.5% [43]: the observed accumulated shift of periastron is in excellent agreement with GR. Over the years, there have been numerous studies on possible violations of GR using the timing of pulsars [e.g. 14, 41], revealing that pulsars are a great research tool in this field. As a result, many alternative gravity theories have been strongly constrained or even falsified (see [15] for a recent review). Pulsars also provide a way to test the no-hair theorem as well as the cosmic censorship conjecture [21, 32]. More recently, pulsar timing has been exploited for the detection of the low-frequency gravitational wave universe [2] through the combination of the timing data for an array of approximately 100 millisecond pulsars (MSP) observed by the largest radio telescopes in the world [44]. Gravitational waves cause changes in the travel times of radio signals between pulsars and the Earth, and a Gravitational Wave Background (GWB) is predicted to produce a specific pattern (the Hellings & Downs curve) in the correlated timing residuals of pairs of pulsars. Generally, any unmodeled effect will appear in the timing residuals: trends in the residuals are indicative of non-optimized parameters, while white

* amodio.carleo@inaf.it

noise residuals with low root-mean-square suggest a good timing model. In the case of a GWB, we expect red noise in the timing residuals at nHz frequencies [12]. In 2023, evidence for a possible GWB was revealed, and looks very promising [1, 13, 36].

A widely adopted timing model that includes all relativistic effects in the dynamics of a binary system up to the first post-Newtonian level is based on Damour and Deruelle’s approach [8] (DD), which has allowed the scientific community to perform self-consistent tests of gravity by means of the parametrised post-Keplerian (PPK) formalism. The main feature of this approach is the closed-form solution of the relativistic first post-Newtonian (PN) two-body problem, making its application immediate. The same approach can be used to incorporate other effects, such as the spin-induced quadrupole moment of the companion [47] and tidal deformations [45], as well as a combination of all these effects. A pseudo-DD formalism can also be adopted, in specific conditions, to include a generic perturbation to Keplerian motion of the form $\Phi(r)_\alpha \propto -Jr^{-\alpha}$, where $J \gg 1$ is the dimensionless perturbation parameter, r the radial coordinate and α the perturbation index [45]. The DD model is therefore the ensemble of pulsar timing formula with the DD description for the binary orbit. In addition to the description of the orbit, which can be Keplerian or post-Keplerian, one usually adopts a post-Newtonian description for the space-time of the binary, in order to account for relativistic effects of the emission time and travel time of the pulsars’ emitted photons. In the weak-field limit, there are different time delays. The three most important ones are: the Roemer delay, the Shapiro delay and the Einstein delay, which need to be taken into account both in the Solar System and in the pulsar binary. In the pulsar binary, the Roemer delay is given by the geometric variation of the distance between the emission point and the observer due to the orbit of the pulsar around the companion. In the Solar System, a similar and additional effect is due to the Earth’s motion around the Sun; in order to avoid the modulation induced by Earth’s orbit, ToAs are referred to the Solar System barycenter (SSB), where coordinate time is defined as $t_{SSB} = t_{em} + (1/c)|\mathbf{r}_p - \mathbf{r}_b|$, where t_{em} is the time of photon emission, and $\mathbf{r}_{p,b}$ is the position of the pulsar or SSB (usually calculated using distant quasars). The Shapiro delay is the (always positive) additional delay that takes into account the deviations of light caused by the gravitational field of the Sun (in the Solar System) and the pulsar’s companion (in the binary); it is easily obtained in the weak-field approximation by solving the geodetic equations and is known up to the 2PN order. Corrections to include lensing and geometric effects are also known [35]. Finally, the Einstein delay is due to the difference between proper time and coordinate time at Earth (in the Solar System) and at the pulsar (in the binary), which is different because of the influence

of the companion’s gravity as well as time dilation. Sometimes, the sum of Roemer and Shapiro delays is called the ‘propagation delay’. These post-Newtonian formulas are widely used by the pulsar community, even if binary pulsars are strong-gravity systems. The reason is that the accuracy of radio data, quantified by the root-mean-square (RMS) value of the timing residuals, although good, is usually not good enough to reveal second-order effects. In exceptional cases, such as in the Double Pulsar system, higher-order corrections to periastron advance and Shapiro delay formulas are necessary [27].

Nowadays, the timing precision of some pulsar experiments has increased from $\sim 10 \mu\text{s}$ to $\sim 100 \text{ ns}$ [46], with good reasons to expect residuals below $\sim 50 \text{ ns}$ in the coming years [19], even near superior conjunction, where accuracy is highly compromised due to eclipses. An accuracy of $\sim 100 \text{ ns}$ or better is also a minimum requirement for detecting a stochastic GWB [42]. Even if software strategies play an important role in precision improvement [46], the real leap in quality will come with the entry into operation of SKA, which could achieve an accuracy of $\sim 10 \text{ ns}$ [30, 39], allowing for extraordinarily accurate measurements of the distance to numerous pulsars, as well as the detection of single sources of nanohertz gravitational waves. One of the goals of SKA is also to detect and perform the timing of pulsars in the galactic center (GC), which is a discovery that has been awaited for many years and which has numerous scientific implications: in addition to an independent measurement of Sgr A*’s mass, pulsar timing analyses in the GC would allow for the measurement of its spin magnitude [49], quadrupole moment [31], the structure of dark matter [20], as well as a series of tests on the geometry of space-time (like the validity of the no-hair theorem [22]) and corresponding gravity tests, given the enormous amplification of any deviations from Einstein’s theory [10, 32]. However, pulsar searches with SKA are not limited to the GC; another main goal is to find, and time, with a similar precision, a pulsar in orbit around a *stellar* black hole [11], which is the type of binary system this paper will focus on.

Given the strong-field regime in the GC region, one wonders whether the usual post-Newtonian timing formulas are valid or not (as compared to the accuracy of the data). All of this forces us to re-evaluate the theoretical framework based, as mentioned above, on a post-Newtonian approximation both for the orbital dynamics and to model the spacetime of the companion object. The question can then be extended to binary systems that are not necessarily extreme (i.e. a supermassive black hole (SMBH) + pulsar), but instead composed of a pulsar and a stellar black hole (BH). The answer to this question is the main goal of this work.

The first evidence for a discrepancy between the full GR treatment and the post-Newtonian approximation

in pulsar timing was covered in [17] and then in [24, 25]. In particular, in [17] an exact analytical formula for the propagation delay in a Schwarzschild space-time is shown. According to this paper, for (nearly) edge-on orbits, the Shapiro delay with a lensing correction deviates quite significantly from the actual, exact propagation delay. For Sgr A*, the maximum difference (superior conjunction) between the exact (analytical) formula and the sum of the single post-Newtonian delays is of ~ 1 s for a pulsar orbiting at distance $r = 10^2 - 10^3$ M, where M is the mass of Sgr A*. When the orbit is inclined, the difference decreases quickly, and arrives at $\sim 10^{-1}$ s for an orbit with the same radius but with an inclination of $\pi/3$. The issue was then further explored in [5], where a comparison between an exact analytical result for the frame-dragging delay (an additional quantity to the propagation delay) and two post-Newtonian derivations for this effect was analyzed. The conclusion is that post-Newtonian based treatments overestimate the frame dragging effect on the light-like signals, in particular around and after superior conjunction, hence the analytical solution provides a more reliable and accurate approach: if the dimensionless spin of Sgr A* is $a = 0.9$, then the best post-Newtonian formula for the frame-dragging delay [35] for a pulsar at $r = 10^3$ M from the SMBH predicts a delay which is 3 s larger than the full GR computation. However, this paper does not report estimates of the total propagation delay, focusing only on the effect of the spin. Later, in [6] the effect of ‘matter’ on the propagation time was investigated using a similar approach, showing that the presence of dark energy around Sgr A* would cause an additional delay of $\simeq 300$ s at superior conjunction (with an advance of $\simeq 40$ s at the inferior conjunction) for SGR J1745-2900, the closest magnetar orbiting Sgr A*. However, at the moment the timing of SGR J1745-2900 has not yet reached sufficient levels of precision for this purpose, mainly due to the intrinsic variability of the source. These papers use an analytical approach to compute the propagation delay, but the necessity of a fully relativistic treatment has also emerged in numerical analyses [25, 49]. A common feature in these works is the assumption of a pulsar orbiting a SMBH, therefore allowing the use of the one-body approximation, since the neutron star is considered as a test particle in the space-time of the black hole. This circumstance, however, in addition to being unique (there is only one supermassive black hole in our galaxy) still does not have an observational counterpart, while the number of pulsars orbiting stellar black holes ($5 - 100 M_\odot$) should be relatively higher, especially in globular clusters [28]. The first discovery of this type may be PSR J0514 - 4002E, an eccentric binary millisecond pulsar in the globular cluster NGC 1851 with a total binary mass of $3.887 \pm 0.004 M_\odot$, i.e. with a companion in the mass gap between a very-massive NS and a low-mass BH [4, 37]. In addition, in globular clusters, we also expect intermediate-mass black holes ($10^2 - 10^5 M_\odot$)

[16], for which post-Newtonian approximations could be not accurate enough.

Here we present the results of an analysis on the discrepancy in the propagation delay (the most substantial part of TOAs) between the usual post-Newtonian formula and a full GR approach, having in mind close-to-discovery systems composed of a pulsar and a stellar or intermediate black hole. The outline of the paper is as follows: in Section 2, we recover the geodesic equations from which the propagation delay is computed; in Section 3, we briefly recall the post-Newtonian formulas; in Section 4, we illustrate our computational algorithm for the full GR computation, with the relativistic case with corrections to the orbital motion discussed in Section 5. We show our results in Section 6 and close the manuscript with a summary and outlook in Section 7.

II. THE PROPAGATION DELAY IN GENERAL RELATIVITY

In this section, we refer to the results in [5, 6, 17] in order to compute the propagation delay in Kerr space-time. This is the time it takes for the radio pulses emitted by a pulsar to reach an observer due to various factors affecting the propagation of the signal through space. This delay is a critical component in precisely measuring the arrival times of pulses and accurately modeling the pulsar’s behavior. In addition to the aforementioned Roemer and Shapiro delays, the propagation of the signal is generally affected by several effects, such as the interaction with free electrons of the interstellar medium (causing the lower-frequency components of the signal to slow down more than the higher-frequency components), with Earth’s ionosphere and the solar wind. Since these are usually smaller effects and, ignoring the transformation from coordinated time to proper time, one usually speaks of ‘propagation delay’ referring mainly to the sum of Roemer and Shapiro delays. In a full GR treatment, such a distinction is not possible and one only solves the photon geodesic equations, obtaining the amount of (coordinate) time required for the pulse to propagate from the NS to the observer in spacetime. About the latter, it is common to consider only the companion object as the source of the stress-energy tensor $T_{\mu\nu}$ to delineate the metric, even if in general both the objects contribute to $T_{\mu\nu}$. In GR, an exact metric for a binary system does not exist due to the non-linearity of the theory and only approximate or numerical solutions can be found. However, if the companion is a black hole, it is sufficient to ignore the mass of the pulsar in the computation of the photon delay. The case of the trajectory of the pulsar itself is different: if the pulsar’s mass is negligible with respect to the companion’s mass, then it moves on time-like geodesics of the companion space-time; if masses are comparable or not so different, then the motion must be

corrected by considering at least 1PN terms.

In order to compute the propagation delay, we focus on the companion object and describe the space-time with a Kerr metric, which is given in Boyer-Lindquist coordinates (t, r, θ, φ) by ($G = c = 1$)

$$ds^2 = -\left(1 - \frac{2Mr}{\Sigma}\right)dt^2 + \frac{\Sigma^2}{\Delta}dr^2 - \frac{2a \sin^2 \theta (2Mr)}{\Sigma^2}d\varphi dt + \Sigma^2 d\theta^2 + \sin^2 \theta \left(r^2 + a^2 + a^2 \sin^2 \theta \frac{2Mr}{\Sigma^2}\right) d\varphi^2 \quad (1)$$

where we defined

$$\Delta \doteq r^2 - 2Mr + a^2, \quad \Sigma^2 \doteq r^2 + a^2 \cos^2 \theta,$$

and M is linked to the mass \bar{M} of the object (likely a black hole) by $\bar{M} = (c^2/G)M$ while $a = J/(Mc)$ where J is its angular momentum. Using the metric components $g_{\mu\nu}$ from the line element ds , geodesic equations are given by

$$g_{\mu\nu} \frac{dx^\mu}{d\tau} \frac{dx^\nu}{d\tau} = \epsilon \quad (2)$$

where τ is an affine parameter and $\epsilon = 0, -1$. While in Schwarzschild space-time orbits starting in the plane (for example $\theta = \pi/2$) remain planar, in Kerr metric this is not true and an additional motion constant is needed: in addition to energy E and angular momentum M , one also needs a separation constant called Carter's constant. Using the Hamilton-Jacobi formalism, we obtain the well-known geodesic equations in Kerr space-time:

$$\dot{t} = \frac{(r^2 + a^2)(r^2 + a^2 - a\lambda)}{\Delta} - a(a - \lambda) + a^2 \cos^2 \theta \quad (3)$$

$$\dot{\varphi} = \frac{a(r^2 + a^2 - a\lambda)}{\Delta} - a + \frac{\lambda}{\sin^2 \theta} \quad (4)$$

$$\dot{\theta}^2 = q + \cos^2 \theta \left[\left(1 + \frac{k}{E^2}\right) a^2 - \frac{\lambda^2}{\sin^2 \theta} \right] = \Theta(\theta) \quad (5)$$

$$\dot{r}^2 = -\Delta \left[q - \frac{k}{E^2} r^2 + (\lambda - a)^2 \right] + (r^2 + a^2 - \lambda a)^2 = R(r). \quad (6)$$

Here, a dot means derivative w.r.t. the so called Mino time γ , which satisfies the condition $dx^\mu = (\Sigma/E)p^\mu d\gamma$, while $q \doteq C/E^2$. Notice that quantities m, E, L, C are constants of motion for the EOMs (3)-(6). For the simplest case of equatorial photon orbits ($q = 0$), the radial potential $R(r)$ has four real roots, namely $r_1 < r_2 < r_3 < r_4$, or at most 2 complex roots, depending on whether the impact parameter λ is greater or smaller than a certain critical value λ_c (one for co-rotating and one for counter-rotating orbits for Kerr metric) corresponding to the so-called unstable spherical or-

bit. The above equations can be analytically solved using elliptic integrals in Legendre form. In particular, combining Eqs. (3), (5) and (6), one gets

$$t_a - t_e = \int_{\gamma_r} \frac{G(r)}{\Delta \sqrt{R(r)}} dr + \int_{\gamma_\theta} \frac{a^2 \cos^2 \theta}{\sqrt{\Theta(\theta)}} d\theta \quad (7)$$

where we have defined

$$G(r) = r^2(r^2 + a^2 + ac(a - \lambda)) + 2Mra(a - \lambda). \quad (8)$$

The integral path γ_r starts at the radial point of emission r_e and either runs monotonically increasing to infinity¹ (direct trajectory) or first decreases in radius towards a turning point outside of the horizons at $r = r_4$ and then continues towards infinity (indirect trajectory). Therefore, the radial integral is split as

$$\left(\int_{r_4}^{\infty} \pm \int_{r_4}^{r_e} \right) \frac{G(r)}{\Delta \sqrt{R(r)}} dr \quad (9)$$

where the minus sign is for a direct trajectory and the plus sign for a flyby motion. Note that when $\lambda < \lambda_c$ only a direct path is possible, while when $\lambda > \lambda_c$ both paths are possible according to the emission position. Neglecting the latitudinal motion (equatorial orbits) and using elliptic integrals, we obtain

$$t_a - t_e = T_r(\infty, \lambda_e) \pm T_r(r_e, \lambda_e) \quad (10)$$

where λ_e is the impact parameter of the emission point and we defined [5, 6, 17]

$$\begin{aligned} T_r(r, \lambda) = & \delta \left[F(x, k) \left(4M^2 \lambda \right. \right. \\ & \left. \left. + 2Mr_3 + \frac{1}{2} [r_1(r_3 - r_4) + r_3(r_3 + r_4)] + \frac{B_+ l}{l_+} + \frac{B_- l}{l_-} \right) \right. \\ & \left. - \frac{1}{2} E(x, k) (r_4 - r_2)(r_3 - r_1) + \Pi(x, l, k) \left(2Mr_4 - 2Mr_3 \right) \right. \\ & \left. + \Pi(x, l_+, k) \left(B_+ - \frac{lB_+}{l_+} \right) + \Pi(x, l_-, k) \left(B_- - \frac{lB_-}{l_-} \right) \right] \\ & + \frac{\sqrt{R(r)}}{r - r_3} \end{aligned} \quad (11)$$

where r_\pm are the horizons, $\delta = 2/\sqrt{(r_4 - r_2)(r_3 - r_1)}$, $l = (r_1 - r_4)/(r_1 - r_3)$, $l_\pm = l(r_3 - r_\pm)/(r_4 - r_\pm)$, and

$$x^2 = \frac{(r - r_4)(r_3 - r_1)}{(r - r_3)(r_4 - r_1)}, \quad k^2 = \frac{(r_3 - r_2)(r_4 - r_1)}{(r_3 - r_1)(r_4 - r_2)},$$

¹ We assume an observer at infinity at $\varphi_a = 0$.

$$B_+ = \frac{8M^3 r_+ - 4a^2 M^2 - 2aM\lambda r_+}{2\sqrt{M^2 - a^2}(r_4 - r_+)}, \quad (12)$$

$$B_- = \frac{-8M^3 r_- + 4a^2 M^2 + 2aM\lambda r_-}{2\sqrt{M^2 - a^2}(r_4 - r_-)}. \quad (13)$$

The functions F , E and Π appearing in Eq. (11) are the well-known elliptic functions of first, second and third kind, respectively. As the propagation delay for an observer at infinity diverges, it is usual to compute the time delay w.r.t. a fixed reference point on the orbit, precisely

$$\Delta t_{ex}(r_e, \varphi_e) = (t_a - t_e) - (t_a - t_{ref})$$

$$= [T_r(\infty, \lambda_e) \pm T_r(r_e, \lambda_e)] - [T_r(\infty, \lambda_{ref}) \pm T_r(r_{ref}, \lambda_{ref})], \quad (14)$$

where λ_{ref} is the angular momentum at the reference point. The ascending node w.r.t. the plane of the sky is usually used as the reference point, as here many post-Newtonian delays are zero.

In order to compute Eq. (10), we need the coordinates of the emission point (r_e, φ_e) in terms of the parameters of the pulsar's orbit as well as its impact parameter λ_e . As pointed out by [17], there is no general analytical solution to such a problem. For the restricted case of equatorial orbits, one needs to numerically solve [6]

$$\varphi_a - \varphi_e = \int_{\gamma_r} \frac{2Mra - a^2\lambda}{\Delta\sqrt{R}(r)} dr + \int_{\gamma_r} \frac{\lambda}{\sqrt{R}(r)_{q=0}} dr. \quad (15)$$

Notice that γ_r includes the points r_e and r_4 : the first can be written as a function of φ_e , while r_4 is known only after fixing a certain λ .

We will consider a binary system composed of a BH of mass M and a pulsar of mass m_p . The relative orbit of the pulsar w.r.t. the black hole (also called 'binary orbit') is an ellipse described by

$$R = a_R(1 - e_R \cos u) \quad (16)$$

where a_R is the semi-major axis, e_R the eccentricity and u the eccentric anomaly. We also consider possible relativistic corrections to the orbital motion; therefore, called $M_{tot} = \bar{M} + m_p$ the total mass, the pulsar orbit is given by $r_p = a_p(1 - e_p \cos u)$ where $a_p = (\bar{M}/M_{tot})a_R$ while e_p is given² by [9]

$$e_p = e_R \left[1 - \frac{Gm_p(m_p - \bar{M})}{2M_{tot}a_R c^2} \right] \quad (17)$$

and similarly for the black hole eccentricity e_c . Note that the azimuthal position φ_e of the pulsar is related to the

true anomaly ϕ (measured from periastron) by [17]

$$\cos \varphi_e = -\sin i \sin(\omega + \phi). \quad (18)$$

where ω is the argument of the periastron and i the inclination of the orbit on the sky plane. In the following, we will also need \mathbf{r}_p and \mathbf{r}_c , namely the positions vectors w.r.t. the binary center-of-mass of the pulsar and BH, respectively. Moreover, we will call \mathbf{n} the unit vector from the binary center-of-mass to the observer.

III. THE POST-NEWTONIAN FORMULA

In the weak-field approximation, the propagation time delay is the sum of Roemer delay [35]

$$\Delta_R = \frac{-\mathbf{n} \cdot \mathbf{r}_p}{c} = \frac{r_p}{c} \sin i \sin(\omega + \phi) \quad (19)$$

(note the dependence on the pulsar's orbit radius) and the 1PN Shapiro delay [29]

$$\Delta_S = \frac{2GM}{c^3} \ln \frac{1 + e_R \cos \phi}{1 - \sin i \sin \psi}. \quad (20)$$

If lensing effect is considered, the latter becomes

$$\Delta_S^{(lens)} = -\frac{2GM}{c^3} \ln \left[\frac{\sqrt{R_{||}^2 + R_{\pm}^2} - R_{||}}{a_R(1 - e_R^2)} \right] \quad (21)$$

where $R_{||} = R \sin i \sin \psi$ is the binary separation along the line of sight and R_{\pm} are the image positions in the sky. The lensing correction to the leading term in the logarithm argument goes as $\sim (GM)/(c^2 a_R)$ [27]. In addition to lensing, there are other delays which are sometimes added in order to capture other GR effects on the propagation of the photons, such as the geometric delay Δ_{geo} [29] and the frame-dragging delay Δ_{FD} [48]. In particular, the first one is given by [35]

$$\Delta_{geo} = \frac{2GM}{c^3} \left[\frac{\Delta b_{\pm}}{R_E} \right]^2 \quad (22)$$

where $R_E = \sqrt{4GM R_{CS} |\sin i|}/c$ is the Einstein radius (R_{CS} being the value of R at the superior conjunction) and $\Delta b_{\pm} = (1/2)(\pm\sqrt{b_0^2 + 4R_E^2} - b_0)$. All of these effects are naturally taken into account in the full GR treatment. Notice that the formulas above use the usual post-Newtonian harmonic coordinates system, which is different from Kerr coordinates [5]. In [17] it was shown that, near superior conjunction, the addition of lensing and geometric effects gives more accurate results (where the distance between the weak-field formulas and the full GR ones) than a 2PN Shapiro delay formula. Furthermore, as we checked, the frame-dragging delay is negligible at the distances we are interested in, namely systems

² For the relation between a_R and binding energy E see Eq. (7.2a) in [9].

with binary separations equal or greater than³ $\sim 10^6 M$, for which the Roemer and Shapiro delays largely dominate. For this reason, in the numerical comparison, we also adopt the simpler prescription (valid for zero spin) $r_{PN} \rightarrow r - M$, where r_{PN} is the radial coordinate in the post-Newtonian approach and $r = R$ the Kerr radial coordinate, in a similar way to what was done in [17] with the difference that here r and r_{PN} are not computed w.r.t. to the center-of-mass but w.r.t. the companion. A final remark is about the so-called retardation effect. As pointed out in [35], the orbital motion of the companion during the crossing of the binary system affects the propagation delay, and hence both $\Delta_S^{(lens)}$ and Δ_{geo} should be corrected. This effect results in the shift of the delay curves by the amount $\sim a_c/c$, where $a_c = (m_p/M_{tot})a_R$ is the semi-major orbit of the companion object, and has been observed only in the Double Pulsar system [27], thanks to high precision data, but it is in general not considered in the literature, therefore we will neglect it. Note that it is not even included in our full GR calculation, as only the use of a ‘boosted’ Kerr/Schwarzschild metric [26] could capture it. However, this is beyond the scope of our work, and it is not essential for the purposes of the estimates we want to find.

IV. THE FULL GR ALGORITHM

Both the propagation delay (14) and the angle variation (15) can be computed using elliptic integrals. In order to evaluate the delay, for each point on the pulsar’s orbit, we need to know the impact parameter λ_e , which is given by the numerical solution of Eq.(15). However, finding this solution is very computationally intensive, therefore we started from an array of values for λ and then for each value, we evaluated the four roots⁴ of the potential $R(r)$, in order to obtain an array of values for $\Delta\varphi = \varphi_a - \varphi_e = -\varphi_e$ through Eq. (15). Since $\mathbf{R} = \mathbf{r}_p - \mathbf{r}_c$, an estimate of the range of λ is given by the geometrical formula [35]

$$\lambda^2 \sim b_0^2 = (\mathbf{n} \times R \times \mathbf{n})^2 = (R \cos \psi)^2 + (R \sin \psi \cos i)^2 \quad (23)$$

where $\psi = w + \phi$. This expression neglects both the retardation effect and the lensing effect (see [35] for details), but this is enough to get a rough estimate of λ once the values of a_R and e_R have been assigned. In fact, a shortcut to avoid the numerical resolution of Eq. (15) could be the direct use of Eq. (23). However, we

found that even at large binary separations, the small difference between b_0 and λ noticeably affects the time delay. Even if $b_0/\lambda \rightarrow 1$ for increasing values of a_R , the absolute difference increases causing a changing in the emission position and hence in the computation of the propagation time delay. In other words, it is not so accurate for our purposes and a complete full GR treatment is the best option. To give an example, in the simpler case of $m_p = 0$, $a_R = 10^6 M$ and $M = 10M_\odot$ the use of b_0 would lead to a maximum absolute difference (at superior conjunction) between the two approaches of $|\Delta t_{ex} - \Delta_R - \Delta_S^{(lens)} - \Delta_{geo} - \Delta_R^{(BH)}| \simeq 10^{-7} \text{ s}$ instead of $\simeq 3 \times 10^{-8} \text{ s}$ found using the GR couple of values (λ, φ_e) . Notice that we need to subtract the Roemer delay of the companion (\mathbf{r}_c instead of \mathbf{r}_p in Eq.(19)), namely $\Delta_R^{(BH)}$, as the latter, in general⁵, is not static and the post-Newtonian Roemer delay is usually computed from the center-of-mass, while Δ_{ex} ‘includes’ a Roemer delay computed from the center of the companion.

In more detail, the algorithm for the GR approach basically works with two modules⁶. With the values of a_R , e_R , m_p , i and w (we will assume $a = 0$) as inputs, and after choosing an appropriate range $\{\lambda_{min}, \lambda_{max}\}$ for λ given by the plotted curve $b_0 = b_0(\varphi_e)$, the first module returns a discrete evaluation of the couples (λ, φ_e) both for direct and indirect trajectories. These couples are used in the second module to compute the exact (GR) propagation time delay (14). We used the ascending node as reference point, which, for an edge-on orbit corresponds to $\varphi_e = \pi/2$. Since it belongs to a direct path, we have

$$T_r(\infty, \lambda_{ref}) \pm T_r(r_{ref}, \lambda_{ref}) \rightarrow T_r(\infty, \lambda_{\bar{\varphi}_e}) - T_r(r_{\bar{\varphi}_e}, \lambda_{\bar{\varphi}_e}) \quad (24)$$

where $\bar{\varphi}_e$ is the closest angle to $\pi/2$ in our discrete list (with a direct trajectory) and $\lambda_{\bar{\varphi}_e}$ and $r_{\bar{\varphi}_e}$ are the corresponding values of impact parameter and radial coordinate. We also assume $w = -\pi/2$ which simplifies Eq. (18); the choice of the periastron position does not affect our order-of-magnitude estimates. As for Δ_{ex} , for each of the delays Δ_R , $\Delta_S^{(lens)}$ and Δ_{geo} we subtract the corresponding delay in the reference point, e.g. $\Delta_R(\lambda, \varphi_e) \rightarrow \Delta_R(\lambda, \varphi_e) - \Delta_R(\lambda_{\bar{\varphi}_e}, \bar{\varphi}_e)$. Note that since we only measure differences in times, the reference point can be any point on the orbit, as long as it is the same for all delays. With the latter, we finally compute the absolute difference

$$\Delta_{DIF} = |\Delta t_{ex} - \Delta_R - \Delta_S^{(lens)} - \Delta_{geo} - \Delta_R^{(BH)}| \quad (25)$$

³ This is the value for the Double Pulsar, for which we assumed $M = 1.3 M_\odot$. The semi-major axis of PSR J0514 – 4002E is $\simeq 10^8 \text{ M}$ and specifically corresponds to 10^{12} cm .

⁴ In our numerical algorithms, we will just consider the case of four real roots, avoiding complex numbers. When necessary, we used interpolation to extract physical quantities.

⁵ Even if we consider the pulsar as a test particle for the propagation delay, its gravitational influence is not neglected for the orbital motion. This approximation of using different approaches for the two cases is common in the literature.

⁶ We used MATHEMATICA 12.2.

which is evaluated at the point closest to the superior conjunction, where we expect the discrepancy to be maximum, especially for highly-inclined orbits. We will sometimes also compute the delay difference far from this portion of the orbit, as for example when the propagation is direct. In this case, we will use

$$\Delta_{DIF} = |\Delta t_{ex} - \Delta_R - \Delta_S - \Delta_{2PN} - \Delta_R^{(BH)}| \quad (26)$$

where Δ_{2PN} is the second order Shapiro delay (see Eq. (32) in [17]).

We conclude this section with a remark on the case of generally inclined orbits, i.e. $i \neq \pi/2$. If $e_R = 0$, the couples (λ, φ_e) found with the first module does not depend⁷ on the inclination angle i (r_e is constant), even if, depending on i , the range of φ_e is limited as $\arccos(\sin i) \leq \varphi_e \leq \arccos(-\sin i)$, meaning that some observation angles $\Delta\varphi$ are not possible. Since we are neglecting the spin to calculate our estimates, we practically find ourselves in a situation of spherical symmetry. Therefore, to compare the two approaches and find the maximum difference when $i \neq \pi/2$, we decided to proceed in the following way: we fix $\phi = \pi$ (superior conjunction), find the corresponding couple (λ, φ_e) and with this we compute the Δ_{ex} . In other words, thanks to the spherical symmetry, when $i \neq \pi/2$ the exact delay at superior conjunction is equivalent to the exact delay of photons with an emission point at $\varphi_e = \pi/2 + i$ on an edge-on orbit. This analogy clearly holds only for circular orbits.

V. THE RELATIVISTIC CASE

While in the previous works [5, 6, 17], the pulsar simply follows a Keplerian orbit, here we generalize by allowing the presence of relativistic corrections to the orbital motion. We encode the latter with the usual dimensionless parameter $\epsilon = (GM_{tot})/(a_R c^2)$ and use the quasi-Newtonian scheme of Damour&Deruelle [7] valid at 1PN. In the relativistic case, the eccentricities of the three orbits (pulsar, black hole, binary) are not the same (see Eq.(17)); however, we still have $r_c + r_p = R$, since $\bar{M}e_p + m_p e_c = M_{tot}e_R$. although there are different ways to describe the relativistic orbit (which is not a closed ellipse) depending on the orbital angle you want to use, the most suitable one is provided by Eq. (16), with the important difference that the relation between the true anomaly ϕ and the eccentric anomaly u is given by [7]

$$\phi = 2q \arctan \left(\frac{1 + e_\theta}{1 - e_\theta} \right)^{1/2} \tan \frac{u}{2} \quad (27)$$

⁷ Obviously, the position of the pulsar along its orbit, which is given by the true anomaly ϕ , does depend on i .

where

$$e_\theta = e_R \left(1 + \frac{\epsilon m_p \bar{M}}{2M_{tot}^2} \right) \quad (28)$$

and $q = 1 + 3\epsilon/(1 - e_R^2)$. To obtain the latter relation, we started from Eq. (4.14) of [7], wrote the binary angular momentum by unit reduced mass, J , as $J = \sqrt{GM_{tot}a_R(1 - e_R^2)}$ and Taylor expanded in ϵ . With this description, the periastron advance is only codified in the constant q , which becomes exactly 1 in the non-relativistic case; we are still allowed to use the constant value $w = -\pi/2$ in Eqs. (18) and (19) and in the definition of ψ , with the caveat that now it corresponds to the periastron angle at a specific (proper or coordinate) reference time.

The numerical algorithm is similar to the non-relativistic case. Given a suitable range for λ , a first module finds the roots r_i and then solves two numerical equations (one for direct and one for indirect trajectory) in the variable $-\pi \leq u \leq \pi$. With this, the angle ϕ (see Eq. (27)) and hence φ_e (see Eq. (4)) are computed. In a second module, the couples (λ, φ_e) are used to find the exact relativistic delay $\Delta_{ex}^{(rel)}$. In this case, we are not interested in the comparison with the weak-field approximations, but we want to test the ability of our algorithm to capture the relativistic corrections to the orbital motion, therefore we compute the quantity

$$\Delta_{relativistic} = \Delta_{ex}^{(rel)} - \Delta_{ex} \quad (29)$$

which is identically zero if $\epsilon = 0$. With this, we can quantify the importance of including the relativistic corrections (1PN) to the orbital motion. Since these corrections are more pronounced in eccentric systems, we will assume $e_R \neq 0$ to evaluate Eq. (29).

VI. RESULTS

In this section, we report the results found with our algorithm to compare the maximum difference (at superior conjunction) between the full GR propagation delay and the sum of the weak-field delays. We first give some estimates for the simple case of $m_p = 0$ (as assumed in previous works). We found that for a pulsar orbiting around a black hole of mass $\bar{M} = 10M_\odot$ on a circular, edge-on orbit of radius $a_R = 10^6 M$, the maximum (at superior conjunction) absolute difference is $\Delta_{DIF} \sim 10^{-7}$ s, which is superior to the predicted precision of SKA. This difference decays quickly as a_R increases: when $a_R = 10^7 M$ it is $\Delta_{DIF} \sim \times 10^{-8}$ s, while $\Delta_{DIF} \sim \times 10^{-9}$ s when $a_R = 10^8 M$. This means that if the stellar BH has a mass of $10M_\odot$, the weak-field approximations will be practically indistinguishable from the full GR formula if $a_R > 10^7 M$. Incidentally, we point out that using b_0 instead of λ would overestimate Δ_{DIF} by a factor of about 10 (when $a_R = 10^6 M$ and it

increases with a_R), demonstrating the fact that having maximum precision on lambda is essential.

In Fig. (1), we show the delay difference Δ_{DIF} for the case of a pulsar with mass $m_p = 2M_\odot$ orbiting a black hole with mass $\bar{M} = 10M_\odot$ on a circular edge-on orbit ($i = \pi/2$) of radius $a_R = 10^6 M \simeq 1.5 \times 10^{12}$ cm and without relativistic corrections, i.e. $\epsilon = 0$. For simplicity we assumed $w = -\pi/2$ and, as mentioned above, this choice does not affect the order of magnitude of our results. By construction, $\Delta_{DIF} \rightarrow 0$ when $\Delta\varphi \rightarrow \frac{\pi}{2}$; for this reason we plotted only a small region around the superior conjunction. As we can see, Δ_{DIF} increases rapidly as the conjunction approaches, reaching an absolute value of $\sim 10^{-7}$ s, mainly due to the discrepancy in the lensing path which is not so accurately computed in the weak-field approximations. For completeness, we also estimated Δ_{DIF} at inferior conjunction, where GR effects on the propagation path are deeply suppressed, and we found $\Delta_{DIF} \sim 10^{-10}$ s which is noticeably smaller (in this case, we used Eq. (26) instead of Eq. (25)).

A more general plot is given in Fig. (2), where we show the results in units of $G\bar{M}/c^3$, i.e. without assuming a priori a mass for the companion. Three different semi-major axis values are displayed, namely $a_R = 10^5 M$, $a_R = 10^6 M$ and $a_R = 10^7 M$. A strong dependence on the mass of the companion appears. For example, if $\bar{M} = 10M_\odot$ and $\Delta\varphi = 3$ (near superior conjunction), then $\Delta_{DIF} \sim 10^{-10}$ s if $a_R \simeq 10^{13}$ cm, $\Delta_{DIF} \sim 10^{-9}$ s if $a_R \simeq 10^{12}$ cm and $\Delta_{DIF} \sim 10^{-8}$ s if $a_R \simeq 10^{11}$ cm, meaning that Δ_{DIF} increases by one order of magnitude if a_R decreases by a similar factor. On the contrary, with a_R fixed, Δ_{DIF} grows linearly with \bar{M} . This is all more clear in Fig. (3), where we show the maximum delay difference in seconds as a function of a_R for different choices of \bar{M} . Since we are only interested in the order of magnitude, we used interpolation on a discrete set of couples (Δ_{DIF}, a_R) . Note that the blue dashed line is for a generic mass, therefore the value on the y-axis must be multiplied by $G\bar{M}c^{-3}$ in cgs units. From this log-log plot we roughly extract a trend for the maximum difference of the type $\Delta_{DIF} \sim k_{\bar{M}} a_R^{-4/3}$ where $k_{\bar{M}}$ is a constant depending only on the mass of the black hole \bar{M} . Indeed, the pulsar's mass m_p is irrelevant for these estimates: different values of m_p certainly imply different orbits for the two objects (and therefore a different propagation delay, see Fig. (4)), however Δ_{DIF} , which is basically a difference between propagation delays, remains practically constant, depending only on a_R and \bar{M} , i.e. on the distance to the companion and on the mass of the latter. Finally, we note that, if the mass \bar{M} is sufficiently large ($100M_\odot$), then Δ_{DIF} is significant ($\sim 10^{-7}$ s) even for large binaries ($a_R \sim 10^{16}$ cm) and that, with the very high value $\bar{M} = 10^5 M_\odot$, Δ_{DIF} increases up to $\sim 10^{-4}$ s.

For the relativistic case (Sec. V), i.e. considering

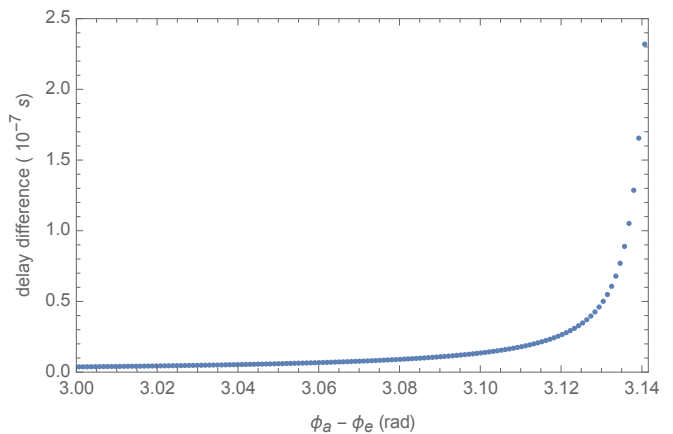


FIG. 1. Delay difference Δ_{DIF} as a function of the observation angle $\Delta\varphi = \varphi_a - \varphi_e \equiv \phi_a - \phi_e$ for the case of a pulsar with mass $m_p = 2M_\odot$ orbiting a black hole with mass $\bar{M} = 10M_\odot$ on a circular edge-on orbit ($i = \pi/2$) of radius $a_R = 10^6 M \simeq 1.5 \times 10^{12}$ cm and without relativistic corrections.

also relativistic corrections to the orbital motion, we assume as a toy model a binary system with $a_R = 10^5 M$, $e_R = 0.5$, $w = -\pi/2$, $i = \pi/2$ and $m_p = 0.2M$. We chose a smaller semi-major axis since we want to emphasize the relativistic contribution. In Fig. (5) we plotted the difference between the exact delay with and without the relativistic corrections (1PN) to the orbital motion, namely Eq. (29). We found that our algorithm is sensitive to relativistic corrections, and these are evident even just considering a single orbit. Depending on the mass of the black hole \bar{M} , the relativistic correction can be very important: for a black hole with $\bar{M} = 10M_\odot$, the relativistic contribution goes up to $\simeq -6.5G\bar{M}c^{-2} \simeq 3.2 \times 10^{-4}$ s. Even if this holds for $a_R = 10^5 M \simeq 0.01$ AU, we conclude that neglecting the relativistic corrections can induce very high errors in the time delay. Moreover, since the periastron advance is a secular effect, we expect that this discrepancy increases with the observation time. Therefore, we recommend always taking into consideration the relativistic contributions, whose importance could be very relevant for future radio telescopes.

Although we expect maximum discrepancies for edge-on orbits, we have also explored cases with a different inclination, in order to decide the importance of using a full GR approach for inclined orbits. We report the results in Table I, where we assumed $a_R = 10^6 M$ and three different masses for the black hole, namely $\bar{M} = 5M_\odot$, $\bar{M} = 10M_\odot$ or $\bar{M} = 100M_\odot$. We deduce that if $\bar{M} = 5M_\odot$ it will be impossible to distinguish the two approaches, except for edge-on orbits. If $\bar{M} = 10M_\odot$, instead, orbits with $75 < i < 90$ could require a full GR computation. Finally, if $\bar{M} = 100M_\odot$, then the discrepancy could be relevant already at low inclinations. Results for different values of a_R scale as discussed above.

Maximum difference delay					
Inclination ($^\circ$)	φ_e (rad)	Δ_{DIF} (GMc^{-3})	Δ_{DIF} (s)	Δ_{DIF} (s)	Δ_{DIF} (s)
15	$\simeq 1.83$	2×10^{-6}	5×10^{-11}	1×10^{-10}	1×10^{-9}
30	$\simeq 2.09$	4×10^{-6}	1×10^{-10}	2×10^{-10}	2×10^{-9}
45	$\simeq 2.35$	8×10^{-6}	2×10^{-10}	4×10^{-10}	4×10^{-9}
60	$\simeq 2.61$	1×10^{-5}	4×10^{-10}	8×10^{-10}	8×10^{-9}
75	$\simeq 2.88$	4×10^{-5}	9×10^{-10}	2×10^{-9}	2×10^{-8}
90	$\simeq 3.14$	5×10^{-3}	1×10^{-7}	2×10^{-7}	2×10^{-6}

TABLE I. Maximum delay difference for different combinations of inclination i and masses \bar{M} of the companion. The third column is in geometric units, while the last three columns are in seconds and for a black hole of mass $5M_\odot$, $10M_\odot$ or $100M_\odot$ respectively. The emission angle φ_e is simply given by $\varphi_e = \frac{\pi}{2} + i$. The other orbital parameters are $a_R = 10^6 M$, $e_R = 0$ and $w_0 = -\pi/2$. The results do not depend on the pulsar mass.

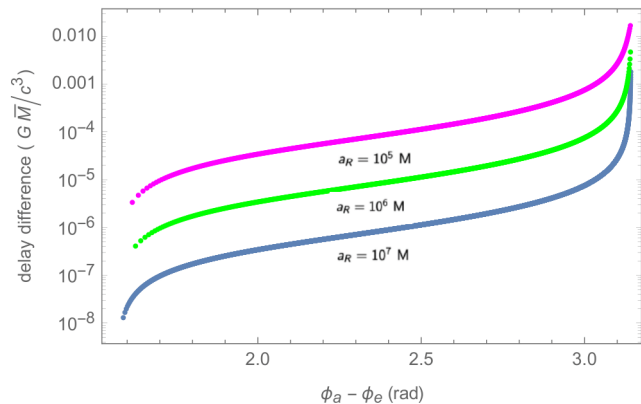


FIG. 2. Delay difference Δ_{DIF} as a function of the observation angle $\Delta\varphi = \varphi_a - \varphi_e \equiv \phi_a - \phi_e$ in units of GM/c^3 for three different values of the semi-major axis of the relative orbit a_R .

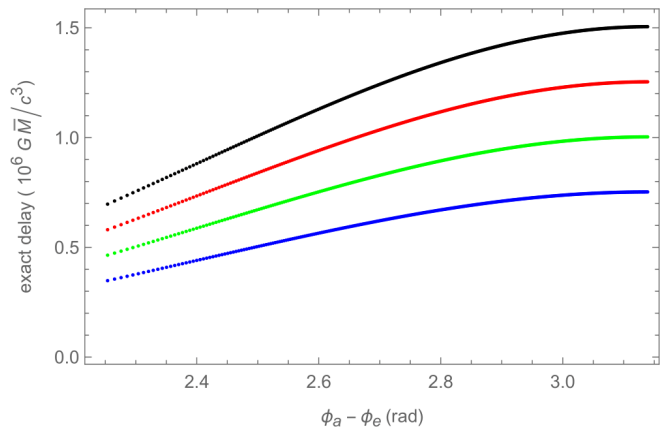


FIG. 4. Exact propagation delay $\Delta t_{ex} - \Delta_R^{(BH)}$ for different values of m_p : 0 (black), $0.2\bar{M}$ (red), $0.5\bar{M}$ and \bar{M} (blue). The other parameters are: $a_R = 10^6 M$, $e_R = 0.5$, $i = \pi/2$, $w_0 = -\pi/2$. The reference point is at $\phi_a - \phi_e = \pi/2$.

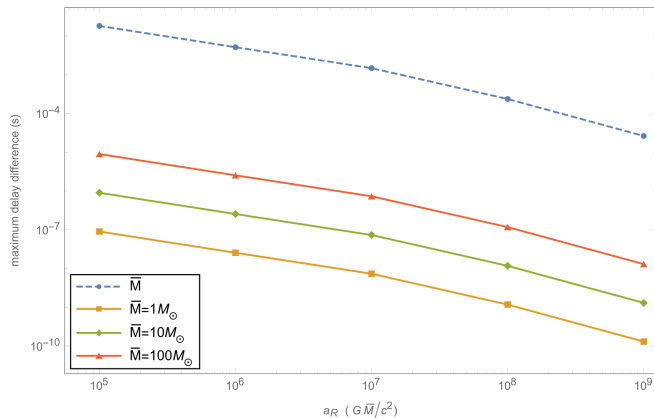


FIG. 3. Log-log plot of the maximum delay difference as a function of the binary semi-major axis a_R for different values of the black hole mass \bar{M} . Interpolation was used on a discrete set of couples (Δ_{DIF}, a_R) . Notice that the blue dashed line is for a generic mass, therefore the value on the y-axis must be multiplied by $GMc^{-3} \simeq 4.4 \times 10^{-5} (\bar{M}/M_\odot)$.

VII. SUMMARY AND OUTLOOK

In the last few years, the timing precision of some pulsar experiments has increased from $\sim 10 \mu\text{s}$ to $\sim 100 \text{ ns}$ [46], with good reasons to expect residuals below $\sim 50 \text{ ns}$ in the coming years [19], even near superior conjunction, where accuracy is highly compromised due to eclipses. Even if software strategies play an important role in precision improvement, the real leap in quality will come with the entry into operation of SKA, which will be able to achieve an accuracy of $\sim 10 \text{ ns}$ [30, 39]. Two important goals of SKA are: (1) to detect and perform the timing of pulsars in the galactic center, which is a discovery that has been awaited for many years and which has numerous scientific implications; (2) to find and time with a great precision a pulsar in orbit around a *stellar* black hole [11], which we expect to find in particular in globular clusters. The strong-field regime in the galactic center region has led us to question whether the usual post-Newtonian formulas used for the timing are still valid. A series of papers [5, 6, 10, 17]

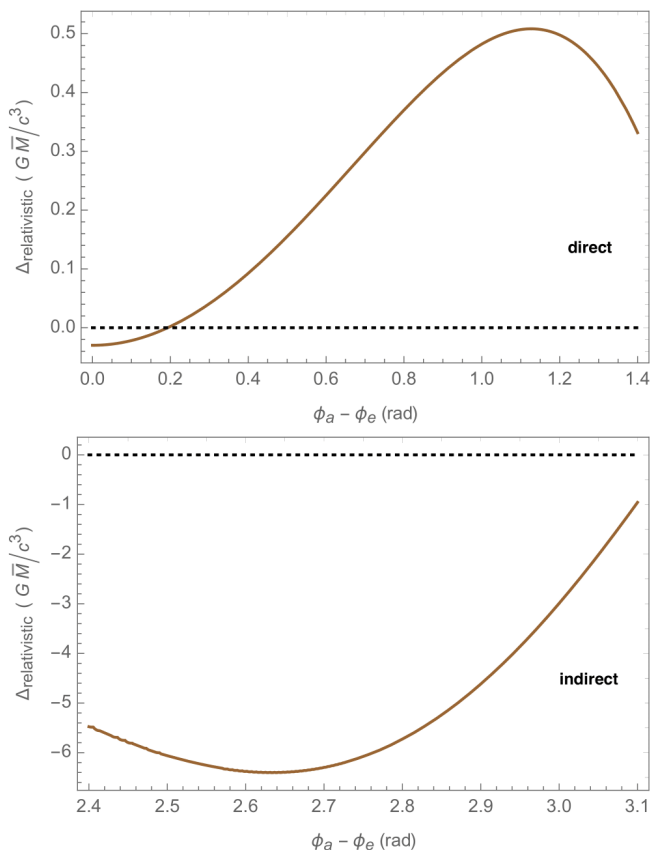


FIG. 5. Difference between the exact delay with and without the relativistic corrections (1PN) to the orbital motion, (see Eq. (29)) as a function of the observation angle. For the binary system we assumed $a_R = 10^5 M$, $e_R = 0.5$, $w = -\pi/2$, $i = \pi/2$ and $m_p = 0.2\bar{M}$, where \bar{M} is the mass of the black hole. (Top) Direct propagation. (Bottom) Indirect propagation.

have confirmed that the timing of a pulsar in the galactic center requires a full GR approach to calculate the propagation delay, especially for edge-on orbits. For Sgr A*, the maximum difference (superior conjunction) between the exact (analytical) formula and the sum of the single post-Newtonian delays is of ~ 1 s for a pulsar orbiting at distance $r = 10^2 - 10^3$ M. A common feature of these works is the assumption of a pulsar orbiting a SMBH, therefore allowing the use of the one-body approximation, since the neutron star is considered as a test particle in the space-time of the black hole. This circumstance, however, in addition to being unique (there is only one supermassive black hole in our galaxy) still does not have an observational counterpart, while the number of pulsars orbiting stellar black holes ($5 - 100 M_\odot$) should be relatively higher, especially in globular clusters [28], where we also expect intermediate-mass black holes ($10^2 - 10^5 M_\odot$) [16], for which the accuracy of the post-Newtonian approximations had not yet been investigated. For these reasons, we have undertaken an analysis on the discrepancy in the propagation delay

(the most substantial part of TOAs) between the usual post-Newtonian formula and a full GR approach, having in mind this close-to-discovery class of systems, i.e. binary pulsars with a stellar or intermediate black hole as a companion. This generalization has made us consider the importance of the orbital motion of the black hole companion. We have therefore corrected the procedure found in these previous works and developed an algorithm to compare the two approaches in the case of these new systems. In addition, we have also considered relativistic corrections to the orbital motion, which have been neglected in the aforementioned works for simplicity.

In more detail, the algorithm for the GR approach basically works with two modules. Given the main orbital parameters as input, the first module returns a discrete evaluation of the impact parameter and emission angle of the photons, while the second module computes the exact (GR) propagation time delay using Eq. (14) and the absolute difference (25) or (26), depending on whether the trajectory is direct or indirect. We found that for a pulsar orbiting a black hole of mass $\bar{M} = 10M_\odot$ on a circular, edge-on orbit of radius $a_R = 10^6 M$, the maximum (at superior conjunction) absolute difference is $\Delta_{DIF} \sim 10^{-7}$ s, which is superior to the predicted precision of SKA, causing non-zero residuals. This difference decays quickly as a_R increases: when $a_R = 10^7 M$ it is $\Delta_{DIF} \sim \times 10^{-8}$ s, while $\Delta_{DIF} \sim \times 10^{-9}$ s when $a_R = 10^8 M$. This means that if the stellar BH has a mass of $10M_\odot$, the weak-field approximations will be practically indistinguishable from the full GR formula if $a_R > 10^7 M$. In general, we found that the difference between the two approaches, Δ_{DIF} , increases by about one order of magnitude if the semi-major axis of the relative orbit, a_R , decreases by a similar factor. More precisely, we roughly extracted a trend for the maximum difference of the type $\Delta_{DIF} \sim k_{\bar{M}} a_R^{-4/3}$, where $k_{\bar{M}}$ is a constant depending only on the mass of the black hole \bar{M} . On the contrary, with a_R fixed, Δ_{DIF} grows linearly with the companion's mass \bar{M} , as clear in Fig. (3), where we show the maximum delay difference (in seconds) as a function of a_R for different choices of \bar{M} . About the pulsar's mass m_p , we discovered that it is basically irrelevant for our estimates on Δ_{DIF} : different values of m_p certainly imply different orbits for the two objects (and therefore a different propagation delay, see Fig. (4)), however Δ_{DIF} , which is a difference between propagation delays, remains practically constant, depending only on a_R and \bar{M} , i.e. on the distance to the companion and on the mass of the latter. This is the result of the theoretical framework adopted in this work and in the previous ones, according to which the pulsar is not considered for the geometry of the space-time in which photons travel; this approximation is always used in the literature due to the lack of an exact analytical metric for binary systems in general relativity. The consequence is that the turning on of the pulsar's mass in the computation of the orbital motions does not

force us to deeply modify the theoretical computation of the propagation delay. The general outline for the comparison with the post-Newtonian prediction remains mostly the same as that of previous works, provided that the parameters of the *relative* orbit are used for the computation of the delay. Speaking of more massive black holes, if the mass \bar{M} is sufficiently large ($100M_\odot$), then Δ_{DIF} is significant ($\sim 10^{-7}$ s) even for large binaries ($a_R \sim 10^{16}$ cm) and, with the very high value $\bar{M} = 10^5 M_\odot$, it increases up to $\sim 10^{-4}$ s. For the relativistic case (see Eq. (29)) instead, we found that, depending on the mass of the black hole \bar{M} , the relativistic correction can be very important: for a black hole with $\bar{M} = 10M_\odot$, the relativistic contribution goes up to $\simeq -6.5G\bar{M}c^{-2} \simeq 3.2 \times 10^{-4}$ s if $a_R = 10^5 M$. Therefore, we conclude that neglecting the relativistic corrections can induce very high errors in the time delay, already in a single-orbit simulation. Since the periastron advance is a secular effect, we expect that this discrepancy increases with the observation time. Finally, although we expect maximum discrepancies for edge-on orbits, we have also explored cases with a different inclination, in order to decide the importance of using a full GR approach for inclined orbits. We report the results in Table I, where we assumed $a_R = 10^6 M$ and three different masses for the black hole, namely $\bar{M} = 5M_\odot$, $\bar{M} = 10M_\odot$ or $\bar{M} = 100M_\odot$. We deduce that if $\bar{M} = 5M_\odot$ it will be impossible to distinguish the two approaches, except for edge-on orbits. If $\bar{M} = 10M_\odot$, instead, orbits with $75 < i < 90$ could require a full GR computation. Finally, if $\bar{M} = 100M_\odot$, then the discrepancy could be relevant even at low inclinations.

There are several ways to extend the results of this work. An important improvement would be the extension of a fully relativistic approach to systems with objects of comparable masses, such as the case of the Double Pulsar. First of all, to calculate the trajectory of the photons, we assumed the space-time as generated only by the companion object. Although this is a usual feature in the field of pulsar timing, this consideration is substantially wrong in cases where the two objects have comparable masses and only works at the 1PN order, where the pulsar's potential introduces a nearly constant delay along the orbit, which is therefore not measurable. However, it is clear that the space-time of relativistic binaries cannot be accurately described by a 1PN 2-body metric, which is not able to capture the complex interaction. On the other hand, i.e. considering a fully analytical approach, it is well known that for binary systems, there are no exact solutions in GR. Therefore, for such systems, we still need to find a middle ground between the 1PN metric (which is not sufficient) and a fully relativistic metric (which does not exist). We ultimately expect that the propagation delay should depend on the pulsar mass and not just the mass of the companion. This can be achieved

by considering approximations of the binary metric that contain interaction terms. Even if it would not be a fully relativistic approach, we believe that this better description of the *binary* space-time may result in non-negligible discrepancies for future timing experiments on systems like the Double pulsar or PSR J0514 – 4002E.

An easier extension, instead, could be the addition of higher-order (2PN) relativistic corrections (only) to the orbital motions, which could have a stronger impact on the accuracy of the timing model than the post-Newtonian approximations of the space-time, since in this work we noticed that the precision at which the emission point along the orbit is known has a huge impact on the evaluation of the delays. Moreover, since relativistic versions of Roemer and Shapiro delays are known [9], it might be fruitful to perform a comparison using them in the post-Newtonian part. However, in this case the need to use eccentric orbits (relativistic effects manifest themselves more in systems with non-zero eccentricity) could complicate the relation between the orbital parameters ($a_R, e_R, a_p, a_c, e_p, e_c, u$) of the post-Newtonian space-time and the corresponding quantities in the Schwarzschild space-time, a task that is immediate when $e_R = 0$ (simply by using the rule $r_{PN} \rightarrow r - M$). A more difficult task might be to use a ‘boosted’ metric [26] instead of the static one used here and in previous papers; this could be far more involved but it would be the only way to include the so-called retardation effect in a full GR calculation of the propagation delay. Finally, we want to point out that the magnitude of Δ_{DIF} is not directly comparable with the timing precision, as the latter is the result of a fit on several parameters depending on several conditions (pulse profile, observation time, signal-to-noise ratio, etc.), therefore the impact of the inaccuracy of the current post-Newtonian formulas on the estimation of the physical quantities (e.g. masses) or on the use of the propagation delay to detect deviations from GR may vary from source to source and it would be useful to quantify it with real cases.

ACKNOWLEDGMENTS

The authors would like to acknowledge the support of the Istituto Nazionale di Astrofisica (INAF). AC thanks Eva Hackmann for several valuable comments. We acknowledge financial support under the National Recovery and Resilience Plan (NRRP), Mission 4, Component 2, Investment 1.1, Call for tender No. 104 published on 2.2.2022 by the Italian Ministry of University and Research (MUR), funded by the European Union - NextGenerationEU - Project Title GUVIRP-Gravity tests in the UltraViolet and InfraRed with Pulsar timing – CUP C53D23000910006 - Grant Assignment Decree No. 962 adopted on 30/06/2023 by the Italian Ministry of University and Research (MUR).

-
- [1] G. Agazie et al. The NANOGrav 15 yr Data Set: Evidence for a Gravitational-wave Background. *Astrophys. J. Lett.*, 951(1):L8, 2023.
- [2] G. Agazie et al. Comparing Recent Pulsar Timing Array Results on the Nanohertz Stochastic Gravitational-wave Background. *Astrophys. J.*, 966(1):105, 2024.
- [3] S. Ascenzi, V. Graber, and N. Rea. Neutron-star measurements in the multi-messenger Era. *Astropart. Phys.*, 158:102935, 2024.
- [4] E. D. Barr, A. Dutta, P. C. C. Freire, M. Cadelano, T. Gautam, M. Kramer, C. Pallanca, S. M. Ransom, A. Ridolfi, B. W. Stappers, T. M. Tauris, V. Venkatraman Krishnan, N. Wex, M. Bailes, J. Behrend, S. Buchner, M. Burgay, W. Chen, D. J. Champion, C.-H. R. Chen, A. Corongiu, M. Geyer, Y. P. Men, P. V. Padmanabh, and A. Possenti. A pulsar in a binary with a compact object in the mass gap between neutron stars and black holes. *Science*, 383(6680):275–279, Jan. 2024.
- [5] B. Ben-Salem and E. Hackmann. Propagation time delay and frame dragging effects of lightlike geodesics in the timing of a pulsar orbiting SgrA*. *Monthly Notices of the Royal Astronomical Society*, 516(2):1768–1780, aug 2022.
- [6] A. Carleo and B. Ben-Salem. Effect of environment in the timing of a pulsar orbiting SgrA*. *Phys. Rev. D*, 108(12):124027, 2023.
- [7] T. Damour and N. Deruelle. General relativistic celestial mechanics of binary systems. I. The post-Newtonian motion. *Annales de L’Institut Henri Poincaré Section (A) Physique Theorique*, 43(1):107–132, Jan. 1985.
- [8] T. Damour and N. Deruelle. General relativistic celestial mechanics of binary systems. II. The post-Newtonian timing formula. *Ann. Inst. Henri Poincaré Phys. Théor.*, 44(3):263–292, Jan. 1986.
- [9] T. Damour and N. Deruelle. General relativistic celestial mechanics of binary systems. II. The post-Newtonian timing formula. *Ann. Inst. Henri Poincaré Phys. Théor.*, Vol. 44, No. 3, p. 263 - 292, 44:263–292, 1986.
- [10] R. Della Monica, I. de Martino, and M. de Laurentis. Testing space–time geometries and theories of gravity at the Galactic centre with pulsar’s time delay. *Mon. Not. Roy. Astron. Soc.*, 524(3):3782–3796, 2023.
- [11] G. Desvignes, R. N. Caballero, L. Lentati, J. P. W. Verbiest, D. J. Champion, B. W. Stappers, G. H. Janssen, P. Lazarus, S. Osłowski, S. Babak, C. G. Bassa, P. Brem, M. Burgay, I. Cognard, J. R. Gair, E. Graikou, L. Guillemot, J. W. T. Hessels, A. Jessner, C. Jordan, R. Karuppusamy, M. Kramer, A. Lassus, K. Lazaridis, K. J. Lee, K. Liu, A. G. Lyne, J. McKee, C. M. F. Mingarelli, D. Perrodin, A. Petiteau, A. Possenti, M. B. Purver, P. A. Rosado, S. Sanidas, A. Sesana, G. Shaifullah, R. Smits, S. R. Taylor, G. Theureau, C. Tiburzi, R. van Haasteren, and A. Vecchio. High-precision timing of 42 millisecond pulsars with the european pulsar timing array. *Monthly Notices of the Royal Astronomical Society*, 458(3):3341–3380, Mar. 2016.
- [12] S. Detweiler. Pulsar timing measurements and the search for gravitational waves. *Astrophys. J.*, 234:1100–1104, Dec. 1979.
- [13] EPTA Collaboration, InPTA Collaboration, J. Antoniadis, P. Arumugam, S. Arumugam, S. Babak, M. Bagchi, A. S. Bak Nielsen, C. G. Bassa, A. Bathula, A. Berthereau, M. Bonetti, E. Bortolas, P. R. Brook, M. Burgay, R. N. Caballero, A. Chalumeau, D. J. Champion, S. Chanlaridis, S. Chen, I. Cognard, S. Dandapat, D. Deb, S. Desai, G. Desvignes, N. Dhanda-Batra, C. Dwivedi, M. Falxa, R. D. Ferdman, A. Franchini, J. R. Gair, B. Goncharov, A. Gopakumar, E. Graikou, J. M. Grießmeier, L. Guillemot, Y. J. Guo, Y. Gupta, S. Hisano, H. Hu, F. Iraci, D. Izquierdo-Villalba, J. Jang, J. Jawor, G. H. Janssen, A. Jessner, B. C. Joshi, F. Kareem, R. Karuppusamy, E. F. Keane, M. J. Keith, D. Kharbanda, T. Kikunaga, N. Kolhe, M. Kramer, M. A. Krishnakumar, K. Lackeos, K. J. Lee, K. Liu, Y. Liu, A. G. Lyne, J. W. McKee, Y. Maan, R. A. Main, M. B. Mickaliger, I. C. Nițu, K. Nobleson, A. K. Paladi, A. Parthasarathy, B. B. P. Perera, D. Perrodin, A. Petiteau, N. K. Porayko, A. Possenti, T. Prabu, H. Quelquejay Leclere, P. Rana, A. Samajdar, S. A. Sanidas, A. Sesana, G. Shaifullah, J. Singha, L. Speri, R. Spiewak, A. Srivastava, B. W. Stappers, M. Surnis, S. C. Susarla, A. Susobhanan, K. Takahashi, P. Tarafdar, G. Theureau, C. Tiburzi, E. van der Wateren, A. Vecchio, V. Venkatraman Krishnan, J. P. W. Verbiest, J. Wang, L. Wang, and Z. Wu. The second data release from the European Pulsar Timing Array. III. Search for gravitational wave signals. *AAP*, 678:A50, Oct. 2023.
- [14] P. C. C. Freire. Tests of gravity theories with pulsar timing, 2022.
- [15] P. C. C. Freire and N. Wex. Gravity experiments with radio pulsars. *Living Reviews in Relativity*, 27(1), July 2024.
- [16] M. S. Fujii, L. Wang, A. Tanikawa, Y. Hirai, and T. R. Saitoh. Simulations predict intermediate-mass black hole formation in globular clusters. *Science*, 384(6703):1488–1492, June 2024.
- [17] E. Hackmann and A. Dhani. The propagation delay in the timing of a pulsar orbiting a supermassive black hole. *General Relativity and Gravitation*, 51(3), mar 2019.
- [18] G. Hobbs, R. Edwards, and R. Manchester. Tempo2, a new pulsar timing package. 1. overview. *Mon. Not. Roy. Astron. Soc.*, 369:655–672, 2006.
- [19] H. Hu, M. Kramer, D. J. Champion, N. Wex, A. Parthasarathy, T. T. Pennucci, N. K. Porayko, W. van Straten, V. Venkatraman Krishnan, M. Burgay, P. C. C. Freire, R. N. Manchester, A. Possenti, I. H. Stairs, M. Bailes, S. Buchner, A. D. Cameron, F. Camilo, and M. Serylak. Gravitational signal propagation in the double pulsar studied with the meerkat telescope. *Astronomy & Astrophysics*, 667:A149, Nov. 2022.
- [20] Z. Hu, L. Shao, and F. Zhang. Prospects for probing small-scale dark matter models with pulsars around Sagittarius A*. *Phys. Rev. D*, 108(12):123034, 2023.
- [21] R. N. Izmailov, E. R. Zhdanov, A. Bhadra, and K. K. Nandi. Relative time delay in a spinning black hole as a diagnostic for no-hair theorem. *Eur. Phys. J. C*, 79(2):105, 2019.
- [22] R. N. Izmailov, E. R. Zhdanov, A. Bhadra, and K. K. Nandi. Relative time delay in a spinning black hole as a diagnostic for no-hair theorem. *European Physical Journal C*, 79(2):105, Feb. 2019.
- [23] M. J. Keith et al. The Thousand-Pulsar-Array pro-

- gramme on MeerKAT – XIII. Timing, flux density, rotation measure, and dispersion measure time series of 597 pulsars. *Mon. Not. Roy. Astron. Soc.*, 530(2):1581–1591, 2024.
- [24] T. Kimpson, K. Wu, and S. Zane. Pulsar timing in extreme mass ratio binaries: a general relativistic approach. *Monthly Notices of the Royal Astronomical Society*, 486(1):360–377, 03 2019.
- [25] Kimpson, T., Wu, K., and Zane, S. Radio timing in a millisecond pulsar - extreme/intermediate mass ratio binary system. *A&A*, 644:A167, 2020.
- [26] S. M. Kopeikin and G. Schäfer. Lorentz covariant theory of light propagation in gravitational fields of arbitrary-moving bodies. *Physical Review D*, 60(12), Nov. 1999.
- [27] M. Kramer, I. Stairs, R. Manchester, N. Wex, A. Deller, W. Coles, M. Ali, M. Burgay, F. Camilo, I. Cognard, T. Damour, G. Desvignes, R. Ferdman, P. Freire, S. Grondin, L. Guillemot, G. Hobbs, G. Janssen, R. Karuppusamy, D. Lorimer, A. Lyne, J. McKee, M. McLaughlin, L. Münch, B. Perera, N. Pol, A. Possenti, J. Sarkissian, B. Stappers, and G. Theureau. Strong-field gravity tests with the double pulsar. *Physical Review X*, 11(4), Dec. 2021.
- [28] K. Kremer, S. Chatterjee, K. Breivik, C. L. Rodriguez, S. L. Larson, and F. A. Rasio. Lisa sources in milky way globular clusters. *Physical Review Letters*, 120(19), May 2018.
- [29] D. Lai and R. R. Rafikov. Effects of gravitational lensing in the double pulsar system J0737-3039. *Astrophys. J.*, 621:L41–L44, 2005.
- [30] K. Liu, J. P. W. Verbiest, M. Kramer, B. W. Stappers, W. van Straten, and J. M. Cordes. Prospects for high-precision pulsar timing: Psr j0437-4715 profile stability. *Monthly Notices of the Royal Astronomical Society*, 417(4):2916–2926, Sept. 2011.
- [31] K. Liu, N. Wex, M. Kramer, J. M. Cordes, and T. J. W. Lazio. Prospects for Probing the Spacetime of Sgr A* with Pulsars. *Astrophys. J.*, 747:1, Mar. 2012.
- [32] K. Liu, N. Wex, M. Kramer, J. M. Cordes, and T. J. W. Lazio. PROSPECTS FOR PROBING THE SPACETIME OF WITH PULSARS. *The Astrophysical Journal*, 747(1):1, feb 2012.
- [33] J. Luo et al. PINT: A Modern Software Package for Pulsar Timing. *Astrophys. J.*, 911(1):45, 2021.
- [34] D. Nice, P. Demorest, I. Stairs, R. Manchester, J. Taylor, W. Peters, J. Weisberg, A. Irwin, N. Wex, and Y. Huang. Tempo: Pulsar timing data analysis. Astrophysics Source Code Library, record ascl:1509.002, Sept. 2015.
- [35] R. Rafikov and D. Lai. Effects of gravitational lensing and companion motion on the binary pulsar timing. *Physical Review D*, 73, 12 2005.
- [36] D. J. Reardon, A. Zic, R. M. Shannon, G. B. Hobbs, M. Bailes, V. Di Marco, A. Kapur, A. F. Rogers, E. Thrane, J. Askew, N. D. R. Bhat, A. Cameron, M. Curyło, W. A. Coles, S. Dai, B. Goncharov, M. Kerr, A. Kulkarni, Y. Levin, M. E. Lower, R. N. Manchester, R. Mandow, M. T. Miles, R. S. Nathan, S. Osłowski, C. J. Russell, R. Spiewak, S. Zhang, and X.-J. Zhu. Search for an Isotropic Gravitational-wave Background with the Parkes Pulsar Timing Array. *Astrophys. J. Lett.*, 951(1), July 2023.
- [37] A. Ridolfi, P. C. C. Freire, T. Gautam, S. M. Ransom, E. D. Barr, S. Buchner, M. Burgay, F. Abbate, V. Venkatraman Krishnan, L. Vleeschower, A. Possenti, B. W. Stappers, M. Kramer, W. Chen, P. V. Padmanabh, D. J. Champion, M. Bailes, L. Levin, E. F. Keane, R. P. Breton, M. Bezuidenhout, J.-M. Grießmeier, L. Küinkel, Y. Men, F. Camilo, M. Geyer, B. V. Hugo, A. Jameson, A. Parthasarathy, and M. Serylak. Trapum discovery of 13 new pulsars in ngc 1851 using meerkat. *Astronomy & Astrophysics*, 664:A27, Aug. 2022.
- [38] C. Smarra et al. Constraints on conformal ultralight dark matter couplings from the European Pulsar Timing Array. 5 2024.
- [39] R. Smits, S. J. Tingay, N. Wex, M. Kramer, and B. Stappers. Prospects for accurate distance measurements of pulsars with the square kilometre array: Enabling fundamental physics. *Astronomy & Astrophysics*, 528:A108, Mar. 2011.
- [40] A. Spolon, L. Zampieri, A. Burtovoi, G. Naletto, C. Barbieri, M. Barbieri, A. Patruno, and E. Verroi. Timing analysis and pulse profile of the Vela pulsar in the optical band from Iqueye observations. *Mon. Not. Roy. Astron. Soc.*, 482(1):175–183, 2019.
- [41] I. H. Stairs. Testing general relativity with pulsar timing. *Living Reviews in Relativity*, 6(1), sep 2003.
- [42] B. W. Stappers, E. F. Keane, M. Kramer, A. Possenti, and I. H. Stairs. The prospects of pulsar timing with new-generation radio telescopes and the Square Kilometre Array. *Philosophical Transactions of the Royal Society of London Series A*, 376(2120):20170293, May 2018.
- [43] J. H. Taylor and J. M. Weisberg. Further experimental tests of relativistic gravity using the binary pulsar psr 1913+ 16. *The Astrophysical Journal*, 345:434–450, 1989.
- [44] J. P. W. Verbiest, S. J. Vigeland, N. K. Porayko, S. Chen, and D. J. Reardon. Status report on global pulsar-timing-array efforts to detect gravitational waves. *Results Phys.*, 61:107719, 2024.
- [45] G. Voisin, R. Breton, and C. Summers. A spider timing model: accounting for quadrupole deformations and relativity in close pulsar binaries. *Mon. Not. Roy. Astron. Soc.*, 492(2):1550–1565, 2020.
- [46] J. Wang, J. P. W. Verbiest, G. M. Shaifullah, I. Cognard, L. Guillemot, G. H. Janssen, M. B. Mickaliger, A. Possenti, and G. Theureau. Improving pulsar timing precision through superior time-of-arrival creation. *Astronomy & Astrophysics*, 687:A154, July 2024.
- [47] N. Wex. A timing formula for main-sequence star binary pulsars. *Mon. Not. Roy. Astron. Soc.*, 298:67, 1998.
- [48] N. Wex and S. M. Kopeikin. Frame Dragging and Other Precessional Effects in Black Hole Pulsar Binaries. *Astrophys. J.*, 514:388–401, Mar. 1999.
- [49] F. Zhang and P. Saha. Probing the spinning of the massive black hole in the galactic center via pulsar timing: A full relativistic treatment. *The Astrophysical Journal*, 849(1):33, Oct. 2017.